Title:

Lumbar corticospinal tract in rodents modulates sensory inputs but does not convey motor command

Authors:

Yunuen Moreno-Lopez[1], Charlotte Bichara[1], Gilles Delbecq, Philippe Isope, Matilde Cordero-Erausquin

[1]These authors contributed equally to this work

Affiliation (+ present address):

Institut des Neurosciences Cellulaires et Intégratives, CNRS UPR 3212, Université de Strasbourg

8 Allée du Général Rouvillois
67000 STRASBOURG
France

M.C.E. : https://orcid.org/0000-0002-1623-1773

P.I.: https://orcid.org/0000-0002-0630-5935

Y.M.L.'s present address: Burke Neurological Institute, White Plains, New York, NY 10605, United States

C.B 's present address: Neuro-Electronics Research Flanders (NERF), 3001 Leuven, Belgium

Corresponding Author :

Matilde Cordero-Erausquin
Tel: (+33) 3 88 45 66 60
Fax: (+33) 3 88 60 16 64
cordero@unistra.fr

Institut des Neurosciences Cellulaires et Intégratives - CNRS UPR 3212
8 allée du Général Rouvillois
67000 Strasbourg cedex, France

Keywords : corticospinal, sensory gating, primary afferent depolarization, motor control

Abstract

It is generally assumed that the main function of the corticospinal tract (CST) is to convey motor commands to bulbar or spinal motoneurons. Yet the CST has also been shown to modulate sensory signals at their entry point in the spinal cord, through presynaptic inhibition. By sequentially investigating different routes of corticofugal pathways through electrophysiological recordings and an intersectional viral strategy, we here demonstrate that motor and sensory modulation commands in mice belong to segregated paths within the CST. Sensory modulation is excuted exclusively by the CST via a population of lumbar interneurons located in the deep dorsal horn. In contrast, the cortex conveys the motor command via a relay in the upper spinal cord or supraspinal motor centers. At lumbar level, the main role of the CST is thus the modulation of sensory inputs, which is an essential component of the selective tuning of sensory feedback, to ensure well-coordinated and skilled movement.

Impact statement

While the corticospinal tract is often considered exclusively as a motor path, this study demonstrates that, in the mouse lumbar cord, its main role is the modulation of sensory inputs.

Text

Introduction

Several brain and spinal structures have been involved in the generation and control of movement, in a task-dependent manner. The primary motor cortex is classically associated to forelimb skilled movements (Starkey et al., 2005; Guo et al., 2015; Miri et al., 2017; Galinanes et al., 2018) and to complex locomotor tasks (obstacles crossing, leaning scale or beam, etc.) (Beloozerova and Sirota, 1993; DiGiovanna et al., 2016; Wang et al., 2017; Bieler et al., 2018) while its role in rythmic locomotion appears, if anything, minor (Beloozerova and Sirota, 1993; DiGiovanna et al., 2016). A coordinated movement relies not only on a proper motor command, but also on the online analysis of an ongoing multi-sensory feedback indicating whether the movement has reached the planned objective or requires correction (Akay et al., 2014; Fink et al., 2014; Azim and Seki, 2019). To optimize the analysis of the overwhelming quantity of reafferent information, specific tuning of peripheral feedback is possible through inhibition of sensory information at different stages of the sensory pathway, a phenomenon known as “sensory gating” (Seki and Fetz, 2012; McComas, 2016).

At the spinal cord level, sensory gating can be mediated by presynaptic inhibition of sensory inputs through primary afferent depolarization (PAD), a powerful mechanism controlled both by supraspinal centers and by adjacent primary afferents (Eccles et al., 1962). While multiple mechanisms have been demonstrated (Shreckengost et al., 2021), the most studied cause of PAD is presynaptic GABA-A mediated depolarization. Primary afferents have indeed a high chloride content and respond to GABA by a depolarization that has been shown to reduce the amplitude of incoming action potentials and thus inhibit synaptic transmission (Prescott and De Koninck, 2003; Doyon et al., 2011). PAD has been involved in the adjustment of reflex excitability (Rudomin and Schmidt, 1999), and its absence results in a pathological context associated with spasticity (Caron et al., 2020). Proprioceptive feedback is required for skilled locomotion (Akay et al., 2014), and presynaptic inhibition of sensory

feedback is essential for performing smooth forelimb skilled movements in mice (Akay et al., 2014; Fink et al., 2014). Interestingly, PAD can also be evoked by stimulation of the sensorimotor cortex in primates, cat and rats (Andersen et al., 1962; Carpenter et al., 1963; Andersen et al., 1964; Abdelmoumene et al., 1970; Eguibar et al., 1994; Wall and Lidierth, 1997). This cortically-evoked PAD may underlie cortical sensory gating at the spinal level and contribute to the cortical involvement in coordinated movements, in addition to the classical drive of motoneurons. In this study, we aimed at elucidating the neuronal pathways conveying the cortical motor command and sensory control to the hindlimb in mice.This cortical control of the spinal cord, either to trigger motoneurons or to modulate sensory information, can rely on multiple pathways, the corticospinal tract (CST) being the most direct one. Its involvement in motor control is long acknowledged, although its precise contribution might vary depending on the motor task (locomotion vs. skilled movement) or targeted limb (forelimb vs. hindlimb) (Miri et al., 2017; Wang et al., 2017; Karadimas et al., 2019). The CST has also been involved in cortically-evoked PAD in cats as a pyramidotomy abolishes it (Rudomin et al., 1986). However, discriminating sensory vs motor contribution has been hampered by the lack of proper tools to segregate functionally or anatomically overlapping paths.

Importantly, none of the CST functions can rely exclusively on direct CST contacts onto motoneurons (MN) as these represent the exception rather than the rule. Indeed, monosynaptic CST-MN contacts are present only in some higher primates, while CST-interneuronal connections are preponderant (in adults) across species (rodents and primates) (Alstermark et al., 2011; Ebbesen and Brecht, 2017; Ueno et al., 2018). In the recent years, specific genetic factors have enabled the identification of several interneuronal populations, and of their inputs, including those from the cortex (Hantman and Jessell, 2010; Bourane et al., 2015; Abraira et al., 2017; Ueno et al., 2018). But neurons with identical genetic markers do not necessary share identical function: in these genetically distinct populations, up to 65% of the neurons receive CST inputs (Ueno et al., 2018), while there is a significant fraction of neurons that is not targeted by the CST. Although manipulating these populations has been extremely informative to better understand their role, it remains unclear whether the changes

observed upon these manipulations can be specifically attributed to the neuronal subset that receives inputs from the CST or to the subset that does not. Therefore, it is still difficult to assess the specific role of the targets of the CST in movements.

In this study, we have investigated the corticofugal paths conveying motor command and modulation of sensory inputs through PAD. We have in particular interrogated the contribution of the CST and its direct lumbar targets through the development of an innovative intersectional viral strategy. We show that cortically-evoked PAD in lumbar primary afferents is conveyed exclusively by the CST through a population of lumbar interneurons. In contrast, our results suggest that motor command to the hindlimbs is relayed either through supraspinal motor centers, or through the CST with a propriospinal relay in the upper cord. The role of the lumbar CST thus appears to be mainly the modulation of sensory inputs, which may in turn selectively increases sensory gain and refines motor control during movement.

Results

PAD and muscular contractions originate in the same cortical area

The rodent sensorimotor cortex has a highly somatotopic organization (Ayling et al., 2009). Mainly studied in a motor perspective, it has been repeatedly mapped for its ability to provoke motor contraction (Li and Waters, 1991; Ayling et al., 2009), but rarely for its ability to induce PAD (Wall and Lidierth, 1997). Cortically-evoked PAD may inhibit the transmission of sensory information from primary afferents to the central nervous system and can be experimentally assessed by recording dorsal root potentials (DRPs, Fig. 1A). We thus recorded DRPs *in vivo* in lumbar roots L4-L6 (conveying hindlimb sensory inputs) of Thy1::ChR2 mice, expressing channelrhodopsin2 in most neuronal cells including layer V cortical neurons (Arenkiel et al., 2007). DRP recordings were performed in isoflurane-

91 anesthetized mice, and trains of photostimulations (5x 8 msec-pulses, 1 msec apart) were applied to
92 activate ChR2 at different positions of the surface of the sensorimotor cortex according to a 500 µm-
93 spaced grid. The area inducing the DRPs was centered at AP=-0.75 mm, L=1.5 mm (Fig. 1C, n=7 mice).
94 Similar photostimulation of this area in mice expressing only the fluorescent reporter EGFP in
95 corticospinal (CS) neurons lead to no DRP signal (see below and Figure 3 – Supplementary figure 1). On
96 a different group of animals, electromyographic (EMG) recordings were performed in the tibialis
97 anterior (*TA*) under ketamine/xylazine anesthesia because EMGs cannot be evoked from cortical
98 stimulation under isoflurane anesthesia (see Methods). The sensorimotor cortex was similarly mapped
99 with trains of photostimulations (6x 1 msec-pulses, 2 msec apart) and the area inducing EMG was
100 centered at : AP=-0.75 mm, L=1.75mm (n=5 mice; Fig. 1C). Again, similar photostimulation of this area
101 in mice expressing only EGFP in CS neurons lead to no EMG signal (see below and Figure 3 –
102 Supplementary figure 1). We observed that the two zones are concentric, demonstrating that
103 cortically-evoked PAD and motor command of the hindlimb can originate from the same cortical area.

104 *Spinal targets of the CST*

105 We next investigated the spinal circuit underlying cortically-evoked DRPs. DRPs can be segmentally-
106 evoked by the activation of a neighboring root, dampening sensory inputs predominantly through
107 GABA-dependent primary-afferent depolarization (Rudomin and Schmidt, 1999). GABAergic terminals
108 presynaptic to proprioceptive fibers arise from GAD65 interneurons (Hughes et al., 2005; Betley et al.,
109 2009) and their activation produces DRPs (Fink et al., 2014). We investigated whether the CST directly
110 targets GAD65-expressing spinal lumbar neurons that could in turn lead to inhibition of primary
111 afferents. In TdTomato-flex mice crossed with GAD65::GFP mice, we injected a monosynaptic
112 anterograde transynaptic virus (AAV1-CBA::WGA-Cre) encoding the Cre-recombinase fused to the
113 wheat germ agglutinin (WGA) (Libbrecht et al., 2017) in the area inducing hindlimb DRPs and EMG
114 (Figure 1 – Figure Supplement 1). The fusion with WGA provides transynaptic properties to the Cre
115 recombinase, which is then transferred to the cortex's monosynaptic targets where it triggers the

116 expression of TdTomato (see Methods, Figure 1 - Figure Supplement 2). We evaluated the proportion
117 of GAD65+ neurons among the spinal targets of the CST revealed by Td-Tomato expression (Fig. 1D-E):
118 16.4±3.2% of spinal Td-Tomato positive neurons were GAD65::GFP+ (69 neurons out of 427, n=3 mice),
119 suggesting that the cortically-evoked DRP may be mediated directly by the activation of a GAD65+
120 spinal target of the CST. In the spinal dorsal horn, cholinergic neurons are a subpopulation of
121 GABAergic neurons (Todd, 1991; Mesnage et al., 2011), and cholinergic terminals are known to be
122 presynaptic to primary afferents (Ribeiro-da-Silva and Cuello, 1990; Pawlowski et al., 2013) and have
123 recently been shown to modulate primary afferent inputs (Hochman et al., 2010; Shreckengost et al.,
124 2021). By performing a similar experiment in ChAT::EGFP mice, we showed that only 2.2±1.8% of CST
125 targets were ChAT::EGFP positive (1 out of 45 neurons, n=4 mice), limiting the likelihood of a direct
126 major involvement of a cholinergic mechanism (Figure 1 - Figure Supplement 3).

127

128 *Segregation of pathways for cortically-evoked DRPs and EMGs*

129 Although lumbar DRPs and tibialis-EMGs (TA-EMGs) are elicited by the same area in the mouse
130 sensorimotor cortex, whether they share the same corticofugal pathway and spinal circuits remains
131 unknown. We first interrogated the contribution of indirect cortical-to-spinal pathways to these two
132 functions (Fig. 2). Since broad photostimulation of the sensorimotor cortex in Thy1::ChR2 activates an
133 heterogeneous population of layer V cortical neurons (Arenkiel et al., 2007) we selectively lesioned the
134 direct CST (Fig. 2B) using an acute electrolytic lesion at the level of the pyramidal decussation
135 (pyramidotomy) (Figure 2 - Figure Supplement 1A, C). In this study, we have consistently performed a
136 caudal pyramidotomy, sparing CST collaterals targeting brainstem motor nuclei that branch more
137 rostrally (Akintunde and Buxton, 1992; Alstermark and Pettersson, 2014) as well as rubrospinal or
138 reticulospinal tracts that can be activated by direct corticorubral or corticoreticular neurons (Fig. 2B).
139 Cortically evoked DRPs were completely abolished by this pyramidotomy (DRP amplitude before: 3.8
140 µV± 0.32 µV; after: 0.30 µV± 0.12 µV , n=3 mice, p=0.006), whereas cortically-evoked EMGs were hardly

141 affected (S/N Ratio 3.3± 0.61 before, 2.2 ± 0.1 after, n=4 mice, p=0.517, all Z-Scores above significance
142 after lesion, Figure 2 - Figure Supplement 2B) (Fig. 2C-D). This demonstrates that indirect cortical-to-
143 spinal pathways (involving supraspinal motor centers) do not encode cortically-evoked DRPs but have
144 a major role for cortically-evoked motor contraction of the hindlimb. These results show that, in the
145 mouse lumbar cord, the CST mediates cortically-evoked DRPs and hence modulates sensory inputs in
146 a presynaptic manner.

147 Although the contribution of the rubrospinal or reticulospinal tracts to motor command is well
148 acknowledged in both rodents and primates, the CST is also believed to encode motor command
149 (Wang et al., 2017). This could have been underrated by simultaneous stimulation of the indirect
150 cortical-to-spinal pathways in Thy1::ChR2 mice. We thus interrogated the specific contribution of the
151 CST to motor contraction by targeting exclusively these neurons through injection of a ChR2-encoding
152 retrograde virus (AAVrg-CAG-hChR2-H134R-tdTomato) in the lumbar spinal cord (Fig. 3A). As expected,
153 the infected CS neurons were located in the area delimited by the previous functional mapping of
154 hindlimb muscle contraction and DRP (Fig. 3B-C). Photostimulation of CS neurons (at the cortical level)
155 induced a robust EMG signal (S/N Ratio 2.4±0.52, n=5 mice, Fig. 3E, upper), demonstrating that CS
156 neurons evoke motor contraction. In agreement with the pyramidotomy results (Fig. 2C), the
157 photostimulation of CS neurons also induced DRPs (mean amplitude = 14.5±4.0µV, n=5), while
158 photostimulation in control mice expressing GFP in CS neurons induced neither an EMG (all Z-Scores
159 below significance) nor a DRP signal (mean amplitude = 0.3±0.0 µV, n=4, Figure 3 – Figure supplement
160 1). Because some CS neurons send collaterals to supraspinal regions involved in motor command
161 (Akintunde and Buxton, 1992), we next addressed whether the motor command traveled through the
162 direct cortical-to-spinal branch of CS neurons or via supraspinal relays. A pyramidotomy, similar to the
163 ones performed above (Figure 2 - Figure Supplement 1C), completely abolished the EMG signal evoked
164 by cortically activating CS neurons (S/N Ratio 0.9±0.12; n=3 mice, p=0.013; all Z scores below
165 significance after pyramidotomy, Figure 2 - Figure Supplement 2C) (Fig. 3D-E). This demonstrates that,
166 while supraspinal collaterals of the CST do not trigger motor output, direct spinal branches can drive

167 motor command. However, this contribution does not seem significant when other cortical neurons
168 are co-activated.

169 *Spinal targets of the CST evoke DRPs but not muscular contraction*

170 Because both DRPs and EMGs of a given limb are encoded by the same sensorimotor cortical area and
171 can be conveyed by the spinal branch of the CST, we next interrogated whether these functions are
172 segregated at the spinal level. CS neurons projecting to the lumbar spinal cord can give off collaterals
173 at the cervico-thoracic level (Kamiyama et al., 2015; Karadimas et al., 2019) and contact cervical
174 propriospinal neurons (Ueno et al., 2012; Ni et al., 2014) that in turn project to lumbar motoneurons
175 to relay motor command (Ni et al., 2014). Indeed, many experiments demonstrated that these neurons
176 are involved in segmental coordination (Miller et al., 1975; Nathan et al., 1996; Reed et al., 2006; Reed
177 et al., 2009). In order to test the contribution of the lumbar branch of CS neurons and rule out
178 antidromic stimulation of rostral collaterals, we combined the transynaptic tool used in Figure 1 with
179 an intersectional approach at the lumbar level. We first identified the lumbar segments containing CST
180 targets by using cortical injection of AAV1-CBA::WGA-Cre in TdTomato-flex mice (Fig. 4A): CST targets
181 were concentrated in spinal lumbar segments L2-L3, rostral to the large pools of motoneurons. They
182 were largely located in the dorsal horn (85,4% were dorsal to the central canal), in particular in the
183 contralateral deep dorsal horn (laminae IV to VII) (Fig. 4B, Fig. 4 – Figure supplement 1). Consistently
184 with the monosynaptic nature of the transynaptic labeling, their number was not correlated with the
185 delay between the infection and the histological analysis (Fig. 4 – Figure supplement 1). CST targets
186 were mostly located in the medial zone, lateral to the dorsal funiculus, where CST fibers penetrate the
187 grey matter. We thus combined the cortical injection of AAV1-CBA::WGA-Cre with the spinal (L4)
188 injection of an AAV (AAV9-Ef1a-DIO-ChETA-EYFP) encoding for a Cre-dependent form of ChETA (a ChR2
189 variant (Gunaydin et al., 2010)) (Fig. 4C). ChETA-EYFP expression was therefore restricted to the lumbar
190 targets of the CST (Fig. 4C, D). Our transectional approach induced ChETA-EYFP expression even in the
191 deepest targets of the CST, in the ventral horn (Fig. 4 – Figure supplement 2). There was no ChETA-

192 EYFP labeling in the dorsal funiculus, demonstrating that the intraspinal AAV injection did not lead to
193 retrograde infection of CS neurons (Fig. 4 – Figure supplement 2). Intraspinal injections did not affect
194 the general behavior of mice (e.g. no visible motor deficits nor pain-like behaviors) nor induced long-
195 lasting weight loss. As surface photostimulation of the spinal cord in Thy1::Cre animals produced an
196 EMG signal and directly activated neurons even in the deep dorsal horn (Fig. 4 – Figure supplement 3),
197 we performed an identical photostimulation in the animals expressing ChETA in the targets of the CST.
198 This stimulation induced a spinal LFP observable as deep as 1150 µm from the surface (Fig. 4 – Figure
199 supplement 3). It also induced DRPs in the ipsilateral lumbar root of 8 out of 9 mice (2.93 ± 0.48 µV,
200 n=8 mice, Fig. 4E-G), demonstrating that DRPs can be directly controlled by the CST projecting to the
201 lumbar cord through local interneurons. However, photostimulation of these same lumbar targets of
202 the CST (same animals) failed to elicit hindlimb movements or muscle contraction as attested by EMG
203 recordings (S/N Ratio 1.0±0.02; n=7 mice, Z-Scores below significance, Figure 2 - Figure Supplement
204 2D) (Fig. 4E-G). Together with the results presented in Fig. 3, we can conclude that CS neurons are able
205 to evoke motor contraction by activation of their spinal targets, but that these targets are not located
206 in the lumbar cord but rather at another spinal level. Cortically-evoked DRPs and EMGs thus follow a
207 similar corticofugal pathway that segregates at the spinal level.

208

209 **Discussion**

210 In this study, we have evaluated the contribution of the CST to the cortical control of movements,
211 either through its ability to convey the muscle contraction command or to modulate sensory inputs.
212 We found that the modulation of sensory inputs from the hindlimb (DRP in lumbar sensory roots) is
213 exclusively carried out by the CST via a population of lumbar interneurons located in the deep dorsal
214 horn. In contrast, the cortex induces muscle contraction of the hindlimb (*TA*) through a relay in the
215 upper spinal cord or supraspinal motor centers. The two mechanisms are therefore segregated, and
216 the main role of the lumbar CST appears to be the modulation of sensory inputs.

217 *Reliability of circuit investigations*

218 We have identified the cortical area involved in these two mechanisms through functional means:
219 cortically-evoked DRPs and EMGs. For ethical and technical reasons, most of these recordings were
220 performed on different animals and conditions. First, EMG recordings after cortical stimulation
221 required a light anesthesia level (Tennant et al., 2011), only possible using Ketamine/Xylazine. Such a
222 light anesthesia is not ethically compatible with the large and invasive surgery required for recording
223 cortically-evoked DRPs. DRPs were thus recorded under isoflurane anesthesia under which no
224 cortically-evoked EMG could be recorded. We therefore acknowledged that the cortical zone
225 responsible for DRPs, smaller than the one responsible for EMGs, might have been underestimated
226 by the deeper anesthesia. We thus did not attempt to quantitatively compare EMG vs DRP map
227 extents, but concluded that they partially overlap allowing us to stimulate at the center of two maps.
228 Although the different experimental approaches might also have differentially affected the
229 recruitment threshold for EMG vs DRP, we do not compare these thresholds in between
230 stimulation/recording configurations. Rather, we analyze the amplitude of a given signal (EMG *or*
231 DRP) with a given experimental approach in different animal models (THY1, ChR2-retro,
232 pyramidotomy, transynaptically labeled CS targets).

233 Circuit investigation also rely on the efficiency of pyramidotomies which affect the spinal branch of
234 CS tract while sparing CST collaterals targeting brainstem motor nuclei, that are branching more
235 rostrally (Akintunde and Buxton, 1992). We performed similar pyramidotomies in two different
236 group of mice, either Thy1::ChR2 or ChR2-retro group (Fig. 1, Fig. 2, Fig. 1 - Figure Supplement 3). In
237 the latter group, in which the CST expressed ChR2, we observed a complete loss of cortically-evoked
238 EMGs after pyramidotomy. These results confirm that the pyramidotomy was efficient to block CST-
239 induced EMG. Therefore, the remaining EMG signal after pyramidotomy in Thy1::ChR2 mice is likely
240 the result of a non-CST pathway.

241 Finally, an intriguing result we report is the absence of EMG signal after photostimulating the targets
242 of the CST at the lumbar level. The reliability of this result relies on multiple technical controls. First,
243 the lack of muscle contraction cannot be attributed to damages of spinal microcircuits due to
244 intraspinal AAV injection. None of the mice presented obvious alteration in the behavior nor a long-
245 lasting weight loss. In addition, similar intraspinal injections were performed for the ChR2-retrograde
246 group, and in these animals, EMG was systematically observed after cortical stimulation,
247 demonstrating the integrity of required spinal circuits. Second, the intraspinal AAV injection
248 efficiently infected neurons in the dorsal horn, and even in the dorsal part of the ventral horn, i.e. in
249 an area comprising 97% of the lumbar targets of the CST. Third, the optic fiber positioned at the
250 surface of the cord evoked an intraspinal LFP as deep as 1150 µm in the double-infected mice, but
251 also evoked EGMs in THY1::ChR2 mice, as previously reported (Caggiano et al., 2016). We also
252 demonstrate direct photoactivation of neurons located up to 700 µm from the surface with the short
253 1 ms stimulus used for EMG recordings. As 73% of the targets of the CST are located within 700 µm
254 from the surface, this demonstrate that the large majority of this population can be directly activated
255 by this procedure. Finally, using a similar surface photostimulation with powers equal or lower than
256 in the present study, Caggiano and colleagues were able to induce motor contraction in ChAT::ChR2
257 animals while considering that they were directly activating motoneurons located in the deep ventral
258 horn (Caggiano et al., 2016). We thus consider very likely that the surface illumination we used could
259 reach most of the lumbar CS-postsynaptic neurons, and that the absence of EMG in this situation is
260 biologically relevent.

261 *Anatomical definition of the hindlimb sensorimotor cortex*

262 In our study, the cortical area inducing hindlimb contraction is similar to that previously reported in
263 mice (Li and Waters, 1991; Ayling et al., 2009). This cortical area (centered around 1mm caudal and
264 1,5mm lateral to bregma) spans over the motor cortex and also partly over the primary
265 somatosensory cortex according to some atlases and studies (Kirkcaldie et al., 2012; Liu et al., 2018;

266 Karadimas et al., 2019). We thus use the conservative term “hindlimb sensorimotor cortex”.
267 Interestingly, we found that stimulation of this area also induced PAD at the lumbar level. This
268 overlap might be a specificity of the “hindlimb area” of the cortex (HLA), and may not generalize to
269 the “forelimb areas” (RFA and CFA). Indeed, the CS neurons from the forelimb areas are spatially
270 segregated (forming clusters projecting either to the dorsal or to the intermediate-ventral cervical
271 cord), while those from the HLA are largely intermingled (Olivares-Moreno et al., 2017). In addition,
272 our results demonstrate that the same cortical area is labelled after retrograde tracing from the
273 lumbar cord (Fig. 3C) excluding the existence of a different pool of cortico-lumbar neurons.

274 *Pathways conveying the cortical motor command*

275 Our study concludes that a large fraction of the cortical motor command to the hindlimb is conveyed
276 through non-CST pathways. These could involve the reticular formation or the red nucleus which
277 receive cortical innervation, project directly or indirectly onto spinal motoneurons, and control
278 different parameters of movements (Lavoie and Drew, 2002; Zelenin et al., 2010; Esposito et al.,
279 2014). Our recordings also suggest that the cortex conveys a motor command to the hindlimb
280 through the CST projecting to a non-lumbar spinal segment as direct stimulation of the CS lumbar
281 targets failed to produce muscle contraction. We have discussed above possible technical caveats
282 and concluded that our approach most likely induced activation of the vast majority of the lumbar CS
283 targets labelled by the transynaptic tracing. We cannot rule out that some of these lumbar targets
284 contribute to convey the cortical motor command to the hindlimb but were not labeled in large
285 enough quantities through our transynaptic approach. The efficiency of WGA-Cre transynaptic
286 tracing might be target specific (Libbrecht et al., 2017), and the number of labelled neurons in the
287 spinal cord suggest that not all targets were labeled. However, this would still implicate that these
288 neurons are distinct from the ones involved in the generation of a DRP, and that these two functions
289 use segregated lumbar pathways. While this hypothesis cannot be excluded, the recent report by
290 Karadimas and collaborators (Karadimas et al., 2019) strongly supports the hypothesis that the motor

291 cortical command conveyed by the CST relays in rostral spinal segments. Indeed, they demonstrate
292 that the cortical motor command to the hindlimb can be mediated by CS neurons projecting to the
293 cervical cord, and then relayed by cervical-to-lumbar propriospinal neurons (Karadimas et al., 2019).
294 Although we selectively study CS projecting at least to the lumbar cord (through lumbar retrograde
295 infection), many CS neurons have collaterals at different spinal segments (Kamiyama et al., 2015).
296 Therefore, their photostimulation at the sensorimotor cortex level would activate cervical pathways
297 in addition to lumbar ones.

298 *Pathways conveying the cortical sensory control*

299 Beyond inducing hindlimb muscle contraction, we have characterized the ability of the cortex to
300 induce DRPs, which is a measure of PAD(Wall and Lidierth, 1997). We demonstrate that it is
301 exclusively relayed through the CST and provide some information on spinal interneurons potentially
302 mediating this effect. The most studied mechanism of segmental PAD involves (Prescott and De
303 Koninck, 2003; Doyon et al., 2011)a presynaptic GABAergic last order neuron (mostly expressing
304 GAD65 (Betley et al., 2009)), located in laminae V-VI, under the control of a first order excitatory
305 interneuron which receives peripheral and descending (including cortical) inputs (Eccles et al., 1962;
306 Rudomin and Schmidt, 1999). (Betley et al., 2009)The targets of the CST identified by our
307 transynaptic labeling are indeed predominantly located in laminae IV-VI, and include a small
308 population of GAD65-expressing neurons. They represent a potential substrate for Cx-DRP that
309 would thus not require a spinal first order excitatory interneuron.

310 In addition to the sensorimotor cortex, stimulation of other supraspinal nuclei are known to induce
311 PAD. This is the case of the red nucleus and the reticular formation (Jimenez et al., 1987; Sirois et al.,
312 2013), both of which also receive inputs from the sensorimotor cortex. The corticorubral and
313 corticoreticular tracts were preserved by the pyramydotomy, yet the cortically-induced PAD was
314 completely lost. This strongly suggests that the ability of the red nucleus and reticular formation to
315 induce PAD does not rely on a sensorimotor cortical command. The control of incoming sensory

316 information through PAD plays an important role in the generation of coordinated movements and
317 processing of sensory information, including nociceptive information (McComas, 2016). GAD65-
318 expressing neurons are essential for smoothed forelimb movements (Fink et al., 2014), but whether
319 they require peripheral or cortical information to do so is yet unknown. Similarly, recordings in
320 primates demonstrated that sensory information is inhibited in a modality- and phase-dependent
321 manner during forelimb voluntary movements (Seki et al., 2003, 2009; Seki and Fetz, 2012)
322 suggesting that this inhibition is somehow related to the motor command, but the exact underlying
323 mechanism remains to be elucidated. Importantly, the change in afferent fiber excitability (Wall,
324 1958) accompanying the sensory presynaptic inhibition in primates was even smaller (<2µV) (Seki et
325 al., 2003) than the DRPs we report as a consequence of cortical stimulation, suggesting that Cx-DRPs
326 might be sufficient to significantly impact the transmission of sensory information. Here, we
327 demonstrate that CS neurons from the same sensorimotor cortex area (but not necessarily a single
328 population) are able to relay both motor command and sensory modulation to hindlimb, but through
329 segregated pathways. Future studies on awake animals and/or focusing on specific sensory
330 modalities are needed to further elucidate the timing and specificity of the sensory control we have
331 described.

332 *Significance of the results*

333 In contrast with the present results on hindlimbs, specific stimulation of the CST at the cervical level
334 induces forelimb contraction (Gu et al., 2017), suggesting a direct relay of the cortical motor
335 command at this level (although antidromic activation of a collateral pathway cannot be excluded).
336 Relative to the forelimb, mice do not display an extensive repertoire of skilled hindlimb movements
337 and a difference in the level of cortical control is expected. The functional segregation we report here
338 suggests that, while the sensory control is selectively targeted at the lumbar level, the hindlimb
339 motor command is relayed in the upper cord. The fact that the upper cord (possibly the cervical cord
340 according to (Karadimas et al., 2019)), receiving the motor command from the forelimb sensorimotor

341 cortex, also receives the information of hindlimb motor command offers a substrate for the
342 coordinated control of fore- and hindlimb, which is essential for most, if not all, skilled movements.

343 The organization of the CST greatly differs between species. From an anatomical point of view, this
344 tract travels mainly in the dorsal funiculus in rodents, while it is located in the dorsolateral funiculus
345 in primates, and its projection area within the spinal cord accordingly differs (Lemon, 2008). The
346 evolution of the CST has been linked to the development of the most dexterous movements that can
347 be performed by primates, with the appearance of direct cortico-motoneuronal (CMN) contacts that
348 are absent in rodents. From an evolutionary perspective, it is interesting to note that the lumbar
349 branch of the CST, which will later acquire a direct motor command role (including with direct CMN
350 contacts in primates (Porter, 1985)) is specialized in mice in the modulation of sensory inputs.
351 Importantly, primate CS neurons don't only form CMN contacts but also abundantly project onto
352 spinal interneurons, and the sensory control function of the CST we report has also been proposed in
353 primates (Lemon, 2019). While extrapolation of our results to primates difficult in view of the large
354 species differences, mice are the main and foremost animal model, including for pathologies
355 affecting the CST such as spinal cord injury or amyotrophic lateral sclerosis. Better understanding the
356 differential roles of the mouse CST in the cervical and lumbar cord is thus an essential endeavor to
357 properly interpret data from these models.

358 *Conclusion*

359 Altogether, our results support a segregation of pathways involved in cortically-evoked sensory
360 modulation vs. motor control. The direct CST is able to induce motor contraction, independently of
361 its supraspinal collaterals, through spinal targets possibly located at the cervico-thoracic level.
362 However, we show that motor command is largely mediated by non-CST pathways, most likely
363 cortico-rubral, or -reticular ones. On the other hand, the major and essential role of the lumbar
364 rodent CST appears to be hindlimb sensory modulation at the primary afferent level, through a
365 population of lumbar target neurons whose activation is sufficient to produce DRPs. (Lemon,

366 2008)This forces re-interpretation of previous studies aiming at promoting CST function in a

367 therapeutic perspective, in mouse injury or neurodegenerative models. While most of these studies

368 have exclusively considered motor command aspects, our results provide a new perspective to

369 analyze these efforts by considering the primary role of rodent lumbar CST, i.e. sensory modulation.

MATERIALS AND METHODS

Animal models. This study was carried out in strict accordance with the national and international laws for laboratory animal welfare and experimentation and was approved in advance by the Ethics Committee of Strasbourg (CREMEAS; CEEA35; agreement number/reference protocol: APAFIS# 12982 - 2017122217349941 v3). The following mice strains were used (adult males and females): Thy1::ChR2 (Cg-Tg(Thy1-COP4/EYFP)18Gfng/J, Jackson Laboratory), TdTomato-Flex (*Gt(ROSA)26Sor*$^{tm14(CAG\text{-}tdTomato)Hze}$/J, Jackson Laboratory), ChAT::EGFP(von Engelhardt et al., 2007), GAD65::GFP(Lopez-Bendito et al., 2004). All lines except GAD65::GFP were back-crossed (at least 10 generations) on a CD1 background. GAD65::GFP were on a C57Bl6/J background. The mice were housed in the Chronobiotron facility (UMS3415, CNRS, University of Strasbourg) in accordance with the European convention 2010/63/EU on the protection of animals used for scientific purposes.

Electrophysiological recordings.

EMG recording: Ketamine/Xylazine anesthesia was chosen to minimally affect muscular tone. After the initial anesthesia (150 mg/kg of ketamine, Imalgene 1000 and 10 mg/kg of Xylazine, Rompun 20%), complementary doses of Ketamine were given when the animal was showing signs of awakening (additional doses bridged by short exposure to Isoflurane 1–1.5%)(Tennant et al., 2011). Concentric EMG needle electrodes (Myoline Xp) were inserted in the *tibialis anterior (TA)* muscle of the animals and a ground electrode was inserted in the tail. Responses were collected with a recording amplifier (IR183A, Cygnus technology) in series with a second amplifier (Brownlee Precision, model440). The traces were filtered with a bandwidth of 0.1 Hz–10 kHz, recorded with Spike 2 software (version 8.00, CED, Cambridge, UK), and analyzed off line with Clampfit (pCLAMP, version 10.7) and home-made python routines (WinPython 2.7.10, Python Software Fundation). EMG responses were recorded after cortical or spinal photostimulation (see below), and the response to 3 consecutive stimulations was averaged for analysis. The area under the curve of the rectified average trace was calculated in a

window of 30ms, either 40 ms before (baseline noise, N) or 10 ms after (signal, S) the onset of the stimulation. The EMG response was presented as the S/N ratio. In CST lesion experiments, all S/N ratios were expressed as a % of the control S/N (average of 3 responses before the lesion). The noise level (S/N of 1) was similarly expressed as a % of the above defined control S/N.

DRP recording: Under isofluorane (1.5-2%) anesthesia, the mice spinal cord was fixed with the spinal cord unit of a stereotaxic frame (Narishige instruments). A laminectomy was performed to expose the surface of lumbar L3-L6 spinal cord segments. A dorsal root (L4-L6) was dissected, cut before the DRG, and a rootlet was suctioned with a glass pipet (sometime two rootlets were suctioned together). An agar pool was created on the exposed spinal cord and filled with NaCl 0.9%. The amplifiers/filters/software used were the same as for the EMG recordings. DRPs in response to 60 successive cortical or spinal photostimulations (see below) were averaged for analysis. The amplitude of the response from the onset to the peak was measured using Clampfit 10.0. The amplitude of the noise was similarly measured on a window preceding photostimulation. For spinal photostimulation, DRPs and EMGs recordings of 3 series of photostimulation were averaged.

For electrophysiological recordings, we excluded animals that had a constant decreasing signals (run-down) in otherwise stable conditions. For DRP recordings that required a delicate surgery, animals were excluded from the study if the surgical preparation / recorvery was compromised or if scaring was abnormal after intraspinal AAV injection.

Single Unit extracellular recording: The animal was prepared and anesthetized as for DRP recordings (except the dorsal root dissection). Single-unit extracellular recordings were made with a glass electrode (Harvard Apparatus, Holliston, MA, USA) filled with 0.5M NaCl and 0.06M HEPES, pH adjusted at 7,3 (resistance ~19 MΩ). A motorized micromanipulator (Narishige, Tokyo, Japan) was used to gradually insert the electrode with 4 µm steps. The amplifiers and software used were the same as for the DRP and EMG recordings, but the signal was at 0.1-3 kHz. The signal was analyzed with Python routines for spike detection (amplitude threshold of 0.30 mV) and delay measure (from onset of photostimulation to spike peak).

421

422 **Cortical photostimulation.** Photostimulation of the cortex was performed on anesthetized animals
423 while recording EMG or DRP. For the cortex, a craniotomy of approximately 9mm^2 was performed
424 under stereo microscope on the contralateral side from the recording site. Muscle contraction,
425 measured by EMG, was evoked by photostimulation with a 250 µm-probe (473 nm laser source PSU-
426 III-FDA, 56mW/cm^2) using the following protocol: trains of 6 pulses, 1 ms duration, 2 ms interval; 15 s
427 minimum between each train (Li and Waters, 1991; Carmel and Martin, 2014). Cortically-evoked DRPS
428 typically require trains of electrical stimulations (Andersen et al., 1962, 1964; Eguibar et al., 1994; Wall
429 and Lidierth, 1997), a protocol that we adapted for photostimulation using a 105 µm-probe (460 nm
430 LED source, Prizmatix, 3.36mW/cm^2): trains of 5 pulses of 8 ms, 1 ms interval and 2 s between each
431 train. In both cases, the probe was moved at the surface of the cortex along a 500 µm-spaced grid.
432 Isopotential contour plots were created, using for EMGs the S/N and for DRPs the peak amplitude
433 (both normalized to the largest values in each animal) at each photostimulation point in the cortex,
434 using a linear interpolation on a set of X, Y, Z triples of a matrix. For EMG, only S/N ratio above
435 significance (Z-Score>3, Figure 2 - Figure Supplement 2A) were considered for the analysis. Then the
436 isopotentials contours were superimposed on the metric planes of the top view of the cortex
437 (Kirkcaldie et al., 2012).

438

439 **Spinal cord photostimulation.** Photostimulation of the spinal cord was performed on anesthetized
440 mice after laminectomy (described above for DRPs recordings), using a 1,1 mm probe (LED source, 42
441 mW/cm^2) first placed on the surface of the lumbar spinal cord (on top of the injection site). The
442 stimulation trains were those used for cortical stimulation. If no signal was observed when stimulating
443 on top of the injection site, the optical fiber was then swept rostrally and caudally on top the whole
444 lumbar segment, in order to try and obtain a signal. EMG and DRP recordings were sequentially
445 performed and required to alternate between different types of anesthesia: isoflurane (craniotomy
446 and laminectomy surgery), ketamine/xylazine (EMG recording), isoflurane 1.5–2 % (DRPs recordings).

447 Only the mice filling the two following criteria were kept for analysis: (i) TdTomato$^+$/EYFP$^+$ neurons
448 were found in the stimulated area; (ii) the response was not precisely associated to the onset or offset
449 of optical pulses (which would be expected for a photoelectric artefact).
450 For spinal single-unit extracellular recordings, the photostimulation protocol consisted in either a
451 single 1ms pulse, or in the same train used to test EMG responses (6 pulses, 1 ms duration, 2 ms
452 interval).
453
454 **Pyramidotomy.** Electrolytic lesion of the CST was performed in a subset of THY1::ChR2 and ChR2
455 retrogradely labeled mice, with 200 ms pulses, 30 mA using a constant current stimulator (Digitimer
456 Ltd thorug) through a silver bipolar electrode inserted in the pyramidal decussation (3.5-4 mm caudal
457 to Bregma, 6 mm deep). The brain was removed for histological analysis at the end of the experiment.
458
459 **Cortical and spinal injections.**
460 Brain injections (1.5–2 mm lateral, 0.5–1 mm caudal to Bregma, 0.5 mm deep) were performed as
461 previously described(Cetin et al., 2006) under isoflurane anesthesia (2–3%). Briefly, 90 to 270 nL of
462 virus was injected by manual pressure using a 5 mL syringe coupled to a calibrated glass capillary, under
463 visual control. Spinal injections were performed using a similar manual pressure protocol. The pipette
464 was inserted in the exposed space between two vertebrae (T13-L1, corresponding to spinal L4), as
465 previously described (Tappe et al., 2006). 0.45 µL of virus was injected 300 µm lateral to the midline
466 and 300-400 µm deep. In both cases, Manitol 12.5% was injected i.p. (0.2 – 0.5 ml) after the surgery
467 to enhance vector spread and improve transduction (Tjolsen et al., 1992). After spinal injection,
468 transfected neurons were found on multiple segments centered in L4 (depending on the animals, up
469 to the whole lumbar enlargement).
470 The animals were kept 2 weeks for the retroAAV injections and a minimum 5 weeks for dual injections
471 before in vivo DRPs and/or EMGs recordings or histological analysis. Animals for which post hoc

472 histological analysis demonstrated inappropriate injections coordinates were excluded from the
473 analysis.
474
475 **Viruses.** AAV2/1-CBA-WGA-CRE-WPRE was purchased at the molecular tools platform at the Centre de
476 recherche CERVO (Québec, Canada), and was used at a titer of $8x10^{12}$ vg/ml. AAV-Ef1a-DIO ChETA-
477 EYFP was a gift from Karl Deisseroth (Gunaydin et al., 2010) (Addgene viral prep # 26968-AAV9;
478 http://n2t.net/addgene:26968 ; RRID:Addgene_26968) and was used at a titer of 1×10^{13} vg/mL. AAV-
479 CAG-hChR2-H134R-tdTomato was a gift from Karel Svoboda (Mao et al., 2011) (Addgene viral prep #
480 28017-AAVrg; http://n2t.net/addgene:28017 ; RRID:Addgene_28017), and was used at a titer of
481 7×10^{12} vg/mL. pAAV-hSyn-EGFP was a gift from Bryan Roth (Addgene viral prep # 50465-AAVrg;
482 http://n2t.net/addgene:50465 ; RRID:Addgene_50465) and was used at a titer of 1×10^{13} vg/mL.
483
484 **Histology**
485 Mice were transcardially perfused with PB followed by 4% paraformaldehyde (PFA) in PB 0.1M, or, if
486 histological analysis followed electrophysiological recordings, the brain and spinal cord were post-fixed
487 overnight in PFA 4% in PB 0.1M. Serial 50 µm brain (coronal or sagittal) and spinal (transverse or
488 sagittal) sections were performed on a vibratome (Leica VT1000 S) and mounted using a DAPI staining
489 mounting medium (Vectashield, Vector laboratories).
490
491 **Image analysis.** The extent of the cortical injection site was estimated by measuring the spread of
492 reporter protein fluorescence (TdTomato) in the layer V of the cortex. The intensity of fluorescence
493 was analyzed as previously described(Lorenzo et al., 2008; Mesnage et al., 2011) on evenly spaced (250
494 µm apart) transverse brain sections imaged with a microscope (Axio Imager 2, Zeiss). Briefly, the "Plot
495 Profile" function of ImageJ software (W. Rasband, National Institutes of Health) was used to measure
496 the intensity of fluorescence along the horizontal axis of a 6000x250 µm rectangle containing the layer
497 V of the cortex (Figure 1 - Figure Supplement 1). These values were normalized to the highest intensity

498 for each animal, and used to plot a density map of each injection site. The contour of the injection area
499 was defined as 30% of the maximal intensity, corresponding to the approximate intensity of individual
500 neurons.

501 *Spatial distribution of corticospinal post-synaptic neurons:* Spinal_lumbar sections (50µm) were
502 mounted serially and imaged using a Zeiss epifluorescence microscope or a Leica SP5 II confocal
503 microscope. Images were aligned manually with Photoshop using the central canal and the dorsal
504 funiculus as landmarks. Each labeled neuron was assigned coordinates corresponding to its distance
505 to the center of the central canal (X and Y) and the index of the slice containing it (Z). This was used to
506 calculate the number of labeled neurons every 100 µm x 100 µm bins (XxY) (or 200 µm x200 µm X x Z)
507 in order to build density plots. The neuronal distribution was plotted using the "spline 16" interpolation
508 method of the matplotlib library in a homemade python script.

509

510 **Quantification and statistical analysis**. No prior sample size calculation was performed. The mean and
511 standard deviation of the Noise were measured from the 3 Noise values obtained from each EMG
512 recording, and used to calculate the Z-scores. The Z-score of each EMG response to the stimulation
513 was calculated using the following equation:

514 $$\text{Z-score} = \frac{\text{Signal- mean Noise}}{\text{standard deviation of Noise}}$$

515 A Z-score of 1.96 or 3 corresponding to a significance level of 0.05 or 0.001 was chosen to discriminate
516 significant responses from non-significant ones. The conservative choice of threshold was chosen in
517 agreement with visual inspection of the traces, to ensure that any EMG responses was not simply due
518 to noise. For each tests, the normality and variance equality were verified by SigmaPlot (Version 13,
519 Copyright © 2014 Systat Softwara, Inc) using Shapiro-Wilk and Brown-Forsythe's methods, before we
520 applied the parametric tests. All the data were analyzed using a one-way ANOVA and a post-hoc test
521 was performed only if an effect showed statistical significance. The P-values for multiple comparison
522 were measured using Holm-Sidak's method. Error bars in all Figures represent mean ± s.e.m., *P <

0.05, NS, no statistical significance (P ≥ 0. 05). The power of the tests was systematically attested to be above the desired power of 0.80.

Acknowledgments

We gratefully acknowledge the support from the CNRS and Strasbourg University; University of Strasbourg Institute for Advanced Study (USIAS) and ANR- 13-JSV4-0003-01 grants to MCE; ANR - 15-CE37-0001-01 CeMod, ANR - 19-CE37-0007-03 MultiMod, and ANR - 19-CE16-0019-01 NetOnTime to PI. YML was supported by a postdoctoral fellowships from the Fondation pour la Recherche Médicale (SPF20160936264) and CB was funded by a fellowship from the Ministère de la Recherche and by the ARSLA (Association pour la Recherche sur la SLA). CB was a student of the EURIDOL graduate School of Pain (University of Strasbourg and ANR-17-EURE-0022). We also thank the following for providing/generating specific mouse lines: Gábor Szabó for GAD65::GFP, Jakob von Engelhardt for ChAT::EGFP. We thank Dr. Sophie Reibel-Foisset and the staff of the animal facility (Chronobiotron, UMS 3415 CNRS and Strasbourg University) for technical assistance. We also thank Yves De Koninck, Frédéric Doussau and Didier Desaintjan for critical reading of the manuscript.

References

Abdelmoumene M, Besson JM, Aleonard P (1970) Cortical areas exerting presynaptic inhibitory action on the spinal cord in cat and monkey. Brain Res 20:327-329.

Abraira VE et al. (2017) The Cellular and Synaptic Architecture of the Mechanosensory Dorsal Horn. Cell 168:295-310 e219.

Akay T, Tourtellotte WG, Arber S, Jessell TM (2014) Degradation of mouse locomotor pattern in the absence of proprioceptive sensory feedback. Proc Natl Acad Sci U S A 111:16877-16882.

Akintunde A, Buxton DF (1992) Origins and collateralization of corticospinal, corticopontine, corticorubral and corticostriatal tracts: a multiple retrograde fluorescent tracing study. Brain Res 586:208-218.

Alstermark B, Pettersson LG (2014) Skilled reaching and grasping in the rat: lacking effect of corticospinal lesion. Front Neurol 5:103.

Alstermark B, Pettersson LG, Nishimura Y, Yoshino-Saito K, Tsuboi F, Takahashi M, Isa T (2011) Motor command for precision grip in the macaque monkey can be mediated by spinal interneurons. J Neurophysiol 106:122-126.

Andersen P, Eccles JC, Sears TA (1962) Presynaptic inhibitory action of cerebral cortex on the spinal cord. Nature 194:740-741.

Andersen P, Eccles JC, Sears TA (1964) Cortically Evoked Depolarization of Primary Afferent Fibers in the Spinal Cord. J Neurophysiol 27:63-77.

Arenkiel BR, Peca J, Davison IG, Feliciano C, Deisseroth K, Augustine GJ, Ehlers MD, Feng G (2007) In vivo light-induced activation of neural circuitry in transgenic mice expressing channelrhodopsin-2. Neuron 54:205-218.

562 Ayling OG, Harrison TC, Boyd JD, Goroshkov A, Murphy TH (2009) Automated light-based mapping of
563 motor cortex by photoactivation of channelrhodopsin-2 transgenic mice. Nat Methods 6:219-224.

564 Azim E, Seki K (2019) Gain control in the sensorimotor system. Curr Opin Physiol 8:177-187.

565 Beloozerova IN, Sirota MG (1993) The role of the motor cortex in the control of accuracy of
566 locomotor movements in the cat. J Physiol 461:1-25.

567 Betley JN, Wright CV, Kawaguchi Y, Erdelyi F, Szabo G, Jessell TM, Kaltschmidt JA (2009) Stringent
568 specificity in the construction of a GABAergic presynaptic inhibitory circuit. Cell 139:161-174.

569 Bieler L, Grassner L, Zaunmair P, Kreutzer C, Lampe L, Trinka E, Marschallinger J, Aigner L, Couillard-
570 Despres S (2018) Motor deficits following dorsal corticospinal tract transection in rats: voluntary
571 versus skilled locomotion readouts. Heliyon 4:e00540.

572 Bourane S, Grossmann KS, Britz O, Dalet A, Del Barrio MG, Stam FJ, Garcia-Campmany L, Koch S,
573 Goulding M (2015) Identification of a spinal circuit for light touch and fine motor control. Cell
574 160:503-515.

575 Caggiano V, Cheung VC, Bizzi E (2016) An Optogenetic Demonstration of Motor Modularity in the
576 Mammalian Spinal Cord. Sci Rep 6:35185.

577 Carmel JB, Martin JH (2014) Motor cortex electrical stimulation augments sprouting of the
578 corticospinal tract and promotes recovery of motor function. Front Integr Neurosci 8:51.

579 Caron G, Bilchak JN, Cote MP (2020) Direct evidence for decreased presynaptic inhibition evoked by
580 PBSt group I muscle afferents after chronic SCI and recovery with step-training in rats. J Physiol
581 598:4621-4642.

582 Carpenter D, Lundberg A, Norrsell U (1963) Primary Afferent Depolarization Evoked from the
583 Sensorimotor Cortex. Acta Physiol Scand 59:126-142.

584 Cetin A, Komai S, Eliava M, Seeburg PH, Osten P (2006) Stereotaxic gene delivery in the rodent brain.
585 Nat Protoc 1:3166-3173.

586 DiGiovanna J, Dominici N, Friedli L, Rigosa J, Duis S, Kreider J, Beauparlant J, van den Brand R,
587 Schieppati M, Micera S, Courtine G (2016) Engagement of the Rat Hindlimb Motor Cortex across
588 Natural Locomotor Behaviors. J Neurosci 36:10440-10455.

589 Doyon N, Prescott SA, Castonguay A, Godin AG, Kroger H, De Koninck Y (2011) Efficacy of synaptic
590 inhibition depends on multiple, dynamically interacting mechanisms implicated in chloride
591 homeostasis. PLoS Comput Biol 7:e1002149.

592 Ebbesen CL, Brecht M (2017) Motor cortex - to act or not to act? Nat Rev Neurosci 18:694-705.

593 Eccles JC, Kostyuk PG, Schmidt RF (1962) Central pathways responsible for depolarization of primary
594 afferent fibres. J Physiol 161:237-257.

595 Eguibar JR, Quevedo J, Jimenez I, Rudomin P (1994) Selective cortical control of information flow
596 through different intraspinal collaterals of the same muscle afferent fiber. Brain Res 643:328-333.

597 Esposito MS, Capelli P, Arber S (2014) Brainstem nucleus MdV mediates skilled forelimb motor tasks.
598 Nature 508:351-356.

599 Fink AJ, Croce KR, Huang ZJ, Abbott LF, Jessell TM, Azim E (2014) Presynaptic inhibition of spinal
600 sensory feedback ensures smooth movement. Nature 509:43-48.

601 Galinanes GL, Bonardi C, Huber D (2018) Directional Reaching for Water as a Cortex-Dependent
602 Behavioral Framework for Mice. Cell Rep 22:2767-2783.

603 Gu Z, Kalambogias J, Yoshioka S, Han W, Li Z, Kawasawa YI, Pochareddy S, Liu F, Xu X, Wijeratne HRS,
604 Ueno M, Blatz E, Salomone J, Kumanogoh A, Rasin MR, Gebelein B, Weirauch MT, Sestan N, Martin
605 JH, Yoshida Y (2017) Control of species-dependent cortico-motoneuronal connections underlying
606 manual dexterity. Science 357:400-404.

607 Gunaydin LA, Yizhar O, Berndt A, Sohal VS, Deisseroth K, Hegemann P (2010) Ultrafast optogenetic
608 control. Nat Neurosci 13:387-392.

609 Guo JZ, Graves AR, Guo WW, Zheng J, Lee A, Rodriguez-Gonzalez J, Li N, Macklin JJ, Phillips JW,
610 Mensh BD, Branson K, Hantman AW (2015) Cortex commands the performance of skilled movement.
611 Elife 4:e10774.

612 Hantman AW, Jessell TM (2010) Clarke's column neurons as the focus of a corticospinal corollary
613 circuit. Nat Neurosci 13:1233-1239.

614 Hochman S, Shreckengost J, Kimura H, Quevedo J (2010) Presynaptic inhibition of primary afferents
615 by depolarization: observations supporting nontraditional mechanisms. Ann N Y Acad Sci 1198:140-
616 152.

617 Hughes DI, Mackie M, Nagy GG, Riddell JS, Maxwell DJ, Szabo G, Erdelyi F, Veress G, Szucs P, Antal M,
618 Todd AJ (2005) P boutons in lamina IX of the rodent spinal cord express high levels of glutamic acid
619 decarboxylase-65 and originate from cells in deep medial dorsal horn. Proc Natl Acad Sci U S A
620 102:9038-9043.

621 Jimenez I, Rudomin P, Solodkin M (1987) Mechanisms involved in the depolarization of cutaneous
622 afferents produced by segmental and descending inputs in the cat spinal cord. Exp Brain Res 69:195-
623 207.

624 Kamiyama T, Kameda H, Murabe N, Fukuda S, Yoshioka N, Mizukami H, Ozawa K, Sakurai M (2015)
625 Corticospinal tract development and spinal cord innervation differ between cervical and lumbar
626 targets. J Neurosci 35:1181-1191.

627 Karadimas SK, Satkunendrarajah K, Laliberte AM, Ringuette D, Weisspapir I, Li L, Gosgnach S, Fehlings
628 MG (2019) Sensory cortical control of movement. Nat Neurosci.

629 Kirkcaldie M, Watson c, Paxinos G, Franklin K (2012) Straightening out the mouse neocortex. In:
630 Australian Neuroscience Society Annual Conference. Goald Coast, QLD.

631 Lavoie S, Drew T (2002) Discharge characteristics of neurons in the red nucleus during voluntary gait
632 modifications: a comparison with the motor cortex. J Neurophysiol 88:1791-1814.

633 Lemon R (2019) Recent advances in our understanding of the primate corticospinal system. F1000Res
634 8.

635 Lemon RN (2008) Descending pathways in motor control. Annu Rev Neurosci 31:195-218.

636 Li CX, Waters RS (1991) Organization of the mouse motor cortex studied by retrograde tracing and
637 intracortical microstimulation (ICMS) mapping. Can J Neurol Sci 18:28-38.

638 Libbrecht S, Van den Haute C, Malinouskaya L, Gijsbers R, Baekelandt V (2017) Evaluation of WGA-
639 Cre-dependent topological transgene expression in the rodent brain. Brain Struct Funct 222:717-733.

640 Liu Y, Latremoliere A, Li X, Zhang Z, Chen M, Wang X, Fang C, Zhu J, Alexandre C, Gao Z, Chen B, Ding
641 X, Zhou JY, Zhang Y, Chen C, Wang KH, Woolf CJ, He Z (2018) Touch and tactile neuropathic pain
642 sensitivity are set by corticospinal projections. Nature 561:547-550.

643 Lopez-Bendito G, Sturgess K, Erdelyi F, Szabo G, Molnar Z, Paulsen O (2004) Preferential origin and
644 layer destination of GAD65-GFP cortical interneurons. Cereb Cortex 14:1122-1133.

645 Lorenzo LE, Ramien M, St Louis M, De Koninck Y, Ribeiro-da-Silva A (2008) Postnatal changes in the
646 Rexed lamination and markers of nociceptive afferents in the superficial dorsal horn of the rat.
647 JComp Neurol 508:592-604.

648 Mao T, Kusefoglu D, Hooks BM, Huber D, Petreanu L, Svoboda K (2011) Long-range neuronal circuits
649 underlying the interaction between sensory and motor cortex. Neuron 72:111-123.

McComas AJ (2016) Hypothesis: Hughlings Jackson and presynaptic inhibition: is there a big picture? J Neurophysiol 116:41-50.

Mesnage B, Gaillard S, Godin A, Rodeau JL, Hammer M, von Engelhardt J, Wiseman P, De Koninck Y, Schlichter R, Cordero-Erausquin M (2011) Morphological and functional characterization of cholinergic interneurons of the dorsal horn of the mouse spinal cord. J Comp Neurol 519:3139-3158.

Miller S, Van Der Burg J, Van Der Meche F (1975) Coordination of movements of the hindlimbs and forelimbs in different forms of locomotion in normal and decerebrate cats. Brain Res 91:217-237.

Miri A, Warriner CL, Seely JS, Elsayed GF, Cunningham JP, Churchland MM, Jessell TM (2017) Behaviorally Selective Engagement of Short-Latency Effector Pathways by Motor Cortex. Neuron 95:683-696 e611.

Nathan PW, Smith M, Deacon P (1996) Vestibulospinal, reticulospinal and descending propriospinal nerve fibres in man. Brain 119 (Pt 6):1809-1833.

Ni Y, Nawabi H, Liu X, Yang L, Miyamichi K, Tedeschi A, Xu B, Wall NR, Callaway EM, He Z (2014) Characterization of long descending premotor propriospinal neurons in the spinal cord. J Neurosci 34:9404-9417.

Olivares-Moreno R, Moreno-Lopez Y, Concha L, Martinez-Lorenzana G, Condes-Lara M, Cordero-Erausquin M, Rojas-Piloni G (2017) The rat corticospinal system is functionally and anatomically segregated. Brain Struct Funct 222:3945-3958.

Pawlowski SA, Gaillard S, Ghorayeb I, Ribeiro-da-Silva A, Schlichter R, Cordero-Erausquin M (2013) A novel population of cholinergic neurons in the macaque spinal dorsal horn of potential clinical relevance for pain therapy. J Neurosci 33:3727-3737.

Porter R (1985) The corticomotoneuronal component of the pyramidal tract: corticomotoneuronal connections and functions in primates. Brain Res 357:1-26.

673 Prescott SA, De Koninck Y (2003) Gain control of firing rate by shunting inhibition: roles of synaptic
674 noise and dendritic saturation. Proc Natl Acad Sci U S A 100:2076-2081.

675 Reed WR, Shum-Siu A, Onifer SM, Magnuson DS (2006) Inter-enlargement pathways in the
676 ventrolateral funiculus of the adult rat spinal cord. Neuroscience 142:1195-1207.

677 Reed WR, Shum-Siu A, Whelan A, Onifer SM, Magnuson DS (2009) Anterograde labeling of
678 ventrolateral funiculus pathways with spinal enlargement connections in the adult rat spinal cord.
679 Brain Res 1302:76-84.

680 Ribeiro-da-Silva A, Cuello AC (1990) Choline acetyltransferase-immunoreactive profiles are
681 presynaptic to primary sensory fibers in the rat superficial dorsal horn. J Comp Neurol 295:370-384.

682 Rudomin P, Schmidt RF (1999) Presynaptic inhibition in the vertebrate spinal cord revisited. Exp Brain
683 Res 129:1-37.

684 Rudomin P, Solodkin M, Jimenez I (1986) PAD and PAH response patterns of group Ia- and Ib-fibers to
685 cutaneous and descending inputs in the cat spinal cord. J Neurophysiol 56:987-1006.

686 Seki K, Fetz EE (2012) Gating of sensory input at spinal and cortical levels during preparation and
687 execution of voluntary movement. J Neurosci 32:890-902.

688 Seki K, Perlmutter SI, Fetz EE (2003) Sensory input to primate spinal cord is presynaptically inhibited
689 during voluntary movement. Nat Neurosci 6:1309-1316.

690 Seki K, Perlmutter SI, Fetz EE (2009) Task-dependent modulation of primary afferent depolarization
691 in cervical spinal cord of monkeys performing an instructed delay task. J Neurophysiol 102:85-99.

692 Shreckengost J, Halder M, Mena-Avila E, Garcia-Ramirez DL, Quevedo J, Hochman S (2021) Nicotinic
693 receptor modulation of primary afferent excitability with selective regulation of Adelta-mediated
694 spinal actions. J Neurophysiol 125:568-585.

695 Sirois J, Frigon A, Gossard JP (2013) Independent control of presynaptic inhibition by reticulospinal
696 and sensory inputs at rest and during rhythmic activities in the cat. J Neurosci 33:8055-8067.

697 Starkey ML, Barritt AW, Yip PK, Davies M, Hamers FP, McMahon SB, Bradbury EJ (2005) Assessing
698 behavioural function following a pyramidotomy lesion of the corticospinal tract in adult mice. Exp
699 Neurol 195:524-539.

700 Tappe A, Klugmann M, Luo C, Hirlinger D, Agarwal N, Benrath J, Ehrengruber MU, During MJ, Kuner R
701 (2006) Synaptic scaffolding protein Homer1a protects against chronic inflammatory pain. Nat Med
702 12:677-681.

703 Tennant KA, Adkins DL, Donlan NA, Asay AL, Thomas N, Kleim JA, Jones TA (2011) The organization of
704 the forelimb representation of the C57BL/6 mouse motor cortex as defined by intracortical
705 microstimulation and cytoarchitecture. Cereb Cortex 21:865-876.

706 Tjolsen A, Berge OG, Hunskaar S, Rosland JH, Hole K (1992) The formalin test: an evaluation of the
707 method. Pain 51:5-17.

708 Todd AJ (1991) Immunohistochemical evidence that acetylcholine and glycine exist in different
709 populations of GABAergic neurons in lamina III of rat spinal dorsal horn. Neuroscience 44:741-746.

710 Ueno M, Hayano Y, Nakagawa H, Yamashita T (2012) Intraspinal rewiring of the corticospinal tract
711 requires target-derived brain-derived neurotrophic factor and compensates lost function after brain
712 injury. Brain 135:1253-1267.

713 Ueno M, Nakamura Y, Li J, Gu Z, Niehaus J, Maezawa M, Crone SA, Goulding M, Baccei ML, Yoshida Y
714 (2018) Corticospinal Circuits from the Sensory and Motor Cortices Differentially Regulate Skilled
715 Movements through Distinct Spinal Interneurons. Cell Rep 23:1286-1300 e1287.

716 von Engelhardt J, Eliava M, Meyer AH, Rozov A, Monyer H (2007) Functional characterization of
717 intrinsic cholinergic interneurons in the cortex. JNeurosci 27:5633-5642.

718 Wall PD (1958) Excitability changes in afferent fibre terminations and their relation to slow
719 potentials. J Physiol 142:1-21.

720 Wall PD, Lidierth M (1997) Five sources of a dorsal root potential: their interactions and origins in the
721 superficial dorsal horn. J Neurophysiol 78:860-871.

722 Wang X, Liu Y, Li X, Zhang Z, Yang H, Zhang Y, Williams PR, Alwahab NSA, Kapur K, Yu B, Chen M, Ding
723 H, Gerfen CR, Wang KH, He Z (2017) Deconstruction of Corticospinal Circuits for Goal-Directed Motor
724 Skills. Cell 171:440-455 e414.

725 Zelenin PV, Beloozerova IN, Sirota MG, Orlovsky GN, Deliagina TG (2010) Activity of red nucleus
726 neurons in the cat during postural corrections. J Neurosci 30:14533-14542.

727

Figure Legends

Figure 1. The same cortical area evokes dorsal root potentials and muscular contractions of the hindlimbs.

A. Schematic experimental design for cortically-evoked (Cx-) DRP and EMG recordings elicited by photostimulation of the contralateral sensorimotor cortex of Thy1::ChR2 mice. DRPs correspond to the presynaptic depolarization of primary afferents propagating antidromically to the suction recording electrode containing a lumbar dorsal root, while EMGs are recorded in the *TA* muscle.

B. Representative traces of a cortically-evoked DRP (top red trace, average of 30 sweeps) and EMG (bottom blue trace, average of 3 sweeps) after photostimulation (blue window) of the contralateral cortex.

C. *Left,* Heatmaps of the amplitude of the responses of cortically-evoked DRPs (top) and EMGs (bottom) in % or the maximum response. *Right*, Overlap of the two maps (red: DRP, blue: EMG) presented as isopotential contour plots (three color grades corresponding to 37%, 50% and 63% of maximum value). Coordinates of the cortex are expressed in mm and centered on *Bregma*. M1: primary motor cortex, M2: secondary motor cortex, and S1: primary sensory cortex, according to the Paxinos atlas (Kirkcaldie et al., 2012).

D. Schematic experimental design to identify GAD65-expressing neurons amongst corticospinal neurons targets: AAV1-CBA-WGA-CRE was injected in the sensorimotor cortex of TdTomato-flex X GAD65::GFP mice. Analysis of extend of the injection site is presented in Figure 1 – Figure Supplement 1, and of the monosynaptic nature of the transynaptic tracing in Figure 1 - Figure Supplement 2.

E. Photomicrographs (z projection of confocal images) of a GAD65::GFP mouse lumbar dorsal horn (localization of the view indicated in the inset) after transynaptic labeling from the

752 hindlimb sensorimotor contralateral cortex. A target of the CST (expressing TdTomato after
753 transynaptic transfer of WGA-Cre) also expresses GAD65::GFP. CST: corticospinal tract. Similar
754 experiment in ChAT::EGFP mice is presented in Figure 1 – Figure Supplement 3.

755

756 **Figure 2. The corticospinal tract is essential for cortically-evoked inhibition of primary afferents.**

757 A. *Left*, diagram showing direct and indirect cortical-to-spinal paths. In green: paths potentially
758 activated by photostimulation in the cortex of Thy1::ChR2 mice. *Right*, experimental design.
759 B. *Left*, drawing showing the extent of the pyramidal lesion (in grey, pyx) in the frontal plane
760 (distance to *Bregma* indicated) in two animals whose recordings are respectively illustrated in
761 C and D. *Right*, diagram showing the indirect cortical-to-spinal paths spared by the
762 pyramidotomy. Systematic histological analysis of the pyramidotomies is presented in Figure
763 2 – Figure Supplement 1.
764 C. *Left*, Representative traces of cortically-evoked DRPs recording before (red) and after (grey)
765 CST lesion (average of 30 traces). *Right*, the pyramidotomy abolishes cortically-evoked DRPs
766 (p= 0.006, one-way ANOVA, n= 3 mice). Post-hoc test Holm-Sidak, *P < 0.05
767 D. *Left*, Representative traces of cortically-evoked EMG recording before (blue) and after (grey)
768 pyramidal lesion (average of 3 traces). *Right*, There is no significant change in the S/N ratio of
769 the EMG response before and after the pyramidal lesion (93,8%, 96,9%, 109,3% prior to
770 pyramidotomy to 77.2% after, p=0.517, one-way ANOVA, n= 4 mice). Grey zone: noise level
771 (see Methods). EMG Z-scores for individual mice before and after pyramidotomy are
772 presented in Figure 2 – Figure Supplement 2.

773

774 **Figure 3. The corticospinal tract can encode muscular contractions.**

775 A. *Left*, diagram illustrating corticospinal neurons and their collaterals expressing ChR2 after
776 retrograde infection in the lumbar cord with a ChR2-retro AAV. *Right*, experimental design:

the photostimulation and EMG recording session took place at least 3 weeks after the infection.

B. Sagittal image from the sensorimotor cortex (Lateral= 0.68 mm), showing retrogradely labeled corticospinal neurons (expressing ChR2-TdTomato).

C. Drawing of a cortex top view, showing the localization of retrogradely labeled corticospinal neurons in the 5 animals (solid lines). They are within the area functionally determined as inducing DRPs and EMGs in the hindlimb (dashed lines).

D. *Left*, drawing showing the extent of the pyramidal lesion in the animal whose recordings are illustrated in E. *Right*, diagram showing the supraspinal collaterals of ChR2-expressing CS neurons spared by the pyramidotomy. Systematic histological analysis of the pyramidotomies is presented in Figure 2 – Figure Supplement 1.

E. *Left*, cortically evoked EMG recordings before (blue) and after (grey) the pyramidal lesion. *Right,* the pyramidotomy abolishes cortically-evoked EMG (p=0.012, one-way ANOVA, n= 5 mice). Post-hoc test Holm-Sidak, *P < 0.05. Grey zone: noise level (see Methods). EMG Z-scores for individual mice before and after pyramidotomy are presented in Figure 2 – Figure Supplement 2.

The blue window on recording traces indicates photostimulation. SMC: sensorimotor cortex, BSMN: brain stem motor nuclei, C-Th: cervico-thoracic spinal cord, L-SC: Lumbo-sacral spinal cord.

Figure 4. Lumbar corticospinal postsynaptic neurons encode DRPs but no movements.

A. Experimental design: the targets of the CST are labeled through a transynaptic approach consisting of AAV1-CBA-WGA-CRE injection in the hindlimb sensorimotor cortex of TdTomato-flex mice.

B. Localization of the spinal targets of the CST: heatmap showing the distribution of the neurons in the lumbar cord (6 mm long) projected into the transverse plane (average of 9 mice) (*left*) or horizontal plane (average of 6 mice) (*right*) plane.

C. *Left*, Diagram illustrating that only lumbar direct targets of the CST express CHETA in the following experiment. *Right*, Experimental design: TdTomato-flex mice received an injection of AAV1-CBA-WGA-CRE in the hindlimb sensorimotor cortex and an injection of AAV1-Efl-flex-CHETA-eYFP in the L4 spinal segment.

D. Photomicrographs (z projection of confocal images) from the dorsal horn of the spinal cord (laminae V/VI); the arrows point at two targets of the CST expressing TdTomato+ and CHETA-eYFP.

E. Experimental design illustrating spinal photostimulation of the lumbar targets of the CST.

F. Representative traces of DRP (red trace, average of 60 traces) and EMG (blue trace, average of 3 traces) recordings from the same animal after photostimulation of the lumbar targets of the CST (blue window).

G. Photostimulation of the lumbar targets of the CST induces DRPs (left) but no EMG signal (right). Grey zone: noise level (see Methods). EMG Z-scores for individual mice are presented in Figure 2 – Figure Supplement 2.

SMC: sensorimotor cortex, BSMN: brain stem motor nuclei, C-Th: cervico-thoracic spinal cord, L-SC:Lumbo-sacral spinal cord.

821 **Figure Supplement material:**

822 Figure 1 - Figure Supplement 1. Sensorimotor injection site analyses : cortical layer V fluorescence
823 quantification.

824 Figure 1 - Figure Supplement 2. Monosynaptic transynaptic tracing from the cortex

825 Figure 1 - Figure Supplement 3. Postsynaptic corticospinal neurons do not colocalize with ChAT.

826 Figure 2 - Figure Supplement 1. Histology of the pyramidotomies.

827 Figure 2 Figure Supplement 2. Z-score of individual EMG responses assessing the significance of the
828 corresponding S/N ratio

829 Figure 3 - Figure Supplement 1. DRPs are induced by photostimulation of ChR2-expressing CS
830 neurons (but not by GFP-expressing CS neurons)

831 Figure 4 - Figure Supplement 1. Strategy to label the spinal targets of corticospinal neurons

832 Figure 4 - Figure Supplement 2. Strategy to stimulate exclusively the spinal targets of corticospinal
833 neurons

834 Figure 4 - Figure Supplement 3. Efficacy of the surface spinal photostimulation

835

836

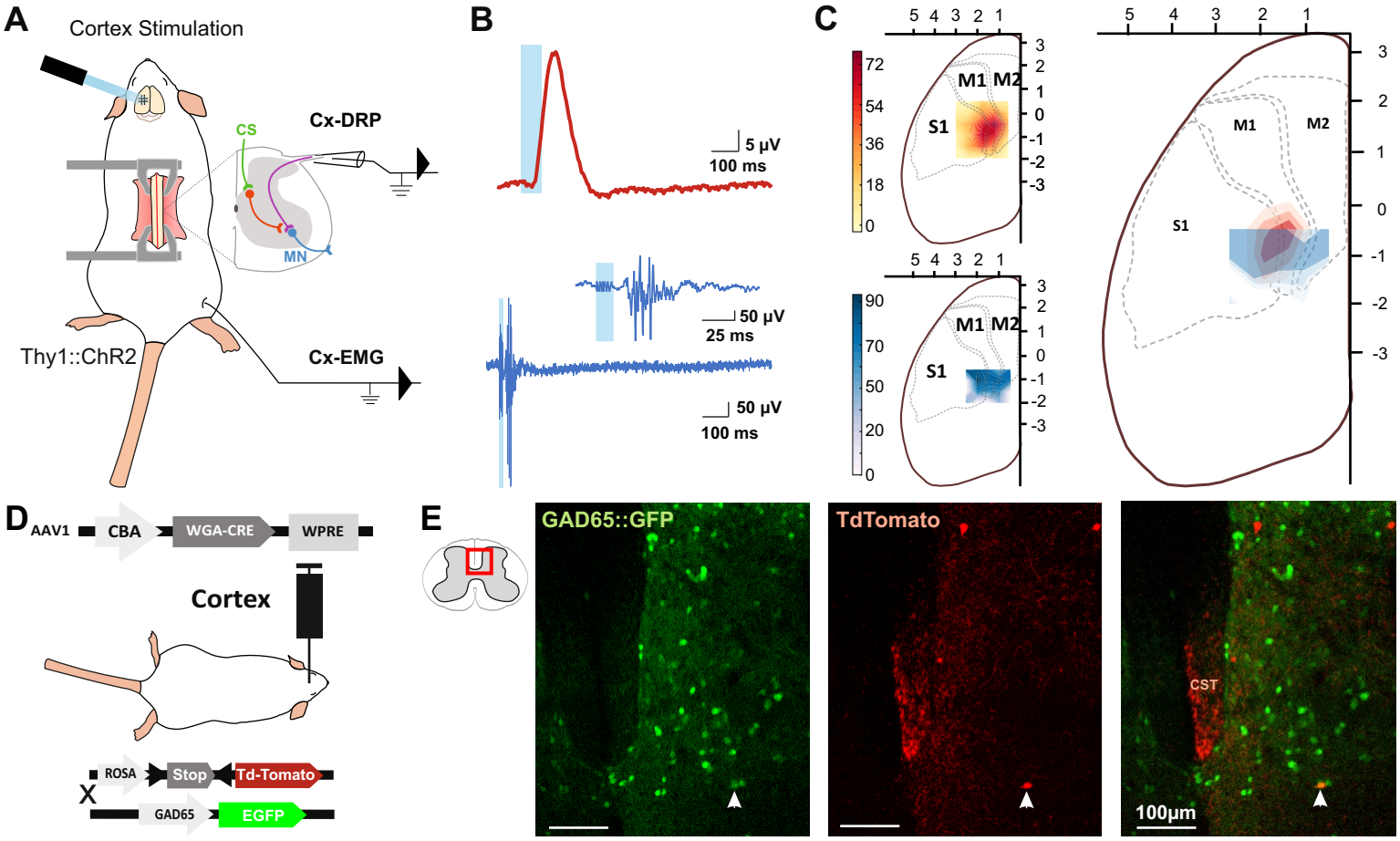

Figure 1. The same cortical area evokes dorsal root potentials and muscular contractions of the hindlimbs.

A. Schematic experimental design for cortically-evoked (Cx-) DRP and EMG recordings elicited by photostimulation of the contralateral sensorimotor cortex of Thy1::ChR2 mice. DRPs correspond to the presynaptic depolarization of primary afferents propagating antidromically to the suction recording electrode containing a lumbar dorsal root, while EMGs are recorded in the *TA* muscle.

B. Representative traces of a cortically-evoked DRP (top red trace, average of 30 sweeps) and EMG (bottom blue trace, average of 3 sweeps) after photostimulation (blue window) of the contralateral cortex.

C. *Left,* Heatmaps of the amplitude of the responses of cortically-evoked DRPs (top) and EMGs (bottom) in % or the maximum response. *Right*, Overlap of the two maps (red: DRP, blue: EMG) presented as isopotential contour plots (three color grades corresponding to 37%, 50% and 63% of maximum value). Coordinates of the cortex are expressed in mm and centered on *Bregma*. M1: primary motor cortex, M2: secondary motor cortex, and S1: primary sensory cortex, according to the Paxinos atlas (Kirkcaldie et al., 2012).

D. Schematic experimental design to identify GAD65-expressing neurons amongst corticospinal neurons targets: AAV1-CBA-WGA-CRE was injected in the sensorimotor cortex of TdTomato-flex X GAD65::GFP mice. Analysis of extend of the injection site is presented in Figure 1 – Figure Supplement. 1, and of the monosynaptic nature of the transynaptic tracing in Figure 1 - Figure Supplement 2.

E. Photomicrographs (z projection of confocal images) of a GAD65::GFP mouse lumbar dorsal horn (localization of the view indicated in the inset) after transynaptic labeling from the hindlimb sensorimotor contralateral cortex. A target of the CST (expressing TdTomato after transynaptic transfer of WGA-Cre) also expresses GAD65::GFP. CST: corticospinal tract. Similar experiment in ChAT::EGFP mice is presented in Figure 1 – Figure Supplement 3.

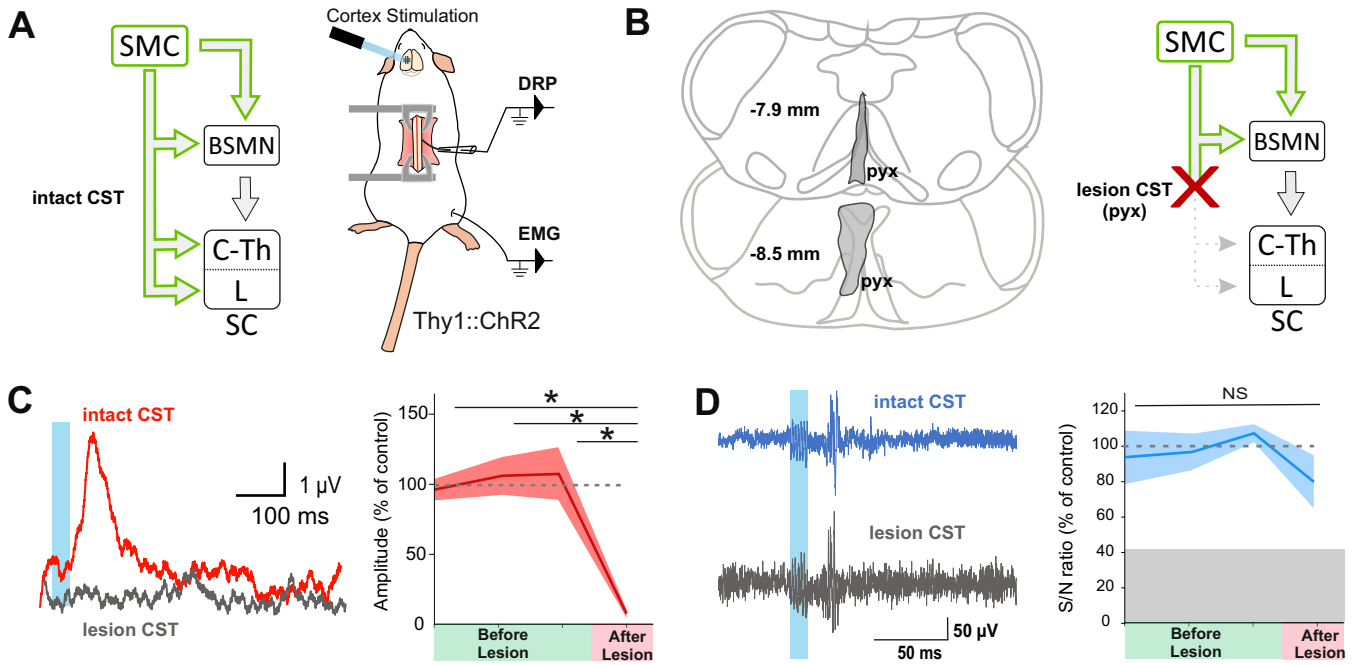

Figure 2. The corticospinal tract is essential for cortically-evoked inhibition of primary afferents.

A. *Left*, diagram showing direct and indirect cortical-to-spinal paths. In green: paths potentially activated by photostimulation in the cortex of Thy1::ChR2 mice. *Right*, experimental design.

B. *Left*, drawing showing the extent of the pyramidal lesion (in grey, pyx) in the frontal plane (distance to *Bregma* indicated) in two animals whose recordings are respectively illustrated in C and D. *Right*, diagram showing the indirect cortical-to-spinal paths spared by the pyramidotomy. Systematic histological analysis of the pyramidotomies is presented in Figure 2 – Figure Supplement 1.

C. *Left*, Representative traces of cortically-evoked DRPs recording before (red) and after (grey) CST lesion (average of 30 traces). *Right*, the pyramidotomy abolishes cortically-evoked DRPs ($p = 0.006$, one-way ANOVA, n= 3 mice). Post-hoc test Holm-Sidak, $*P < 0.05$

D. *Left*, Representative traces of cortically-evoked EMG recording before (blue) and after (grey) pyramidal lesion (average of 3 traces). *Right*, There is no significant change in the S/N ratio of the EMG response before and after the pyramidal lesion ($p=0.517$, one-way ANOVA, n= 4 mice). Grey zone: noise level (see Methods). EMG Z-scores for individual mice before and after pyramidotomy are presented in Figure 2 – Figure Supplement 2.

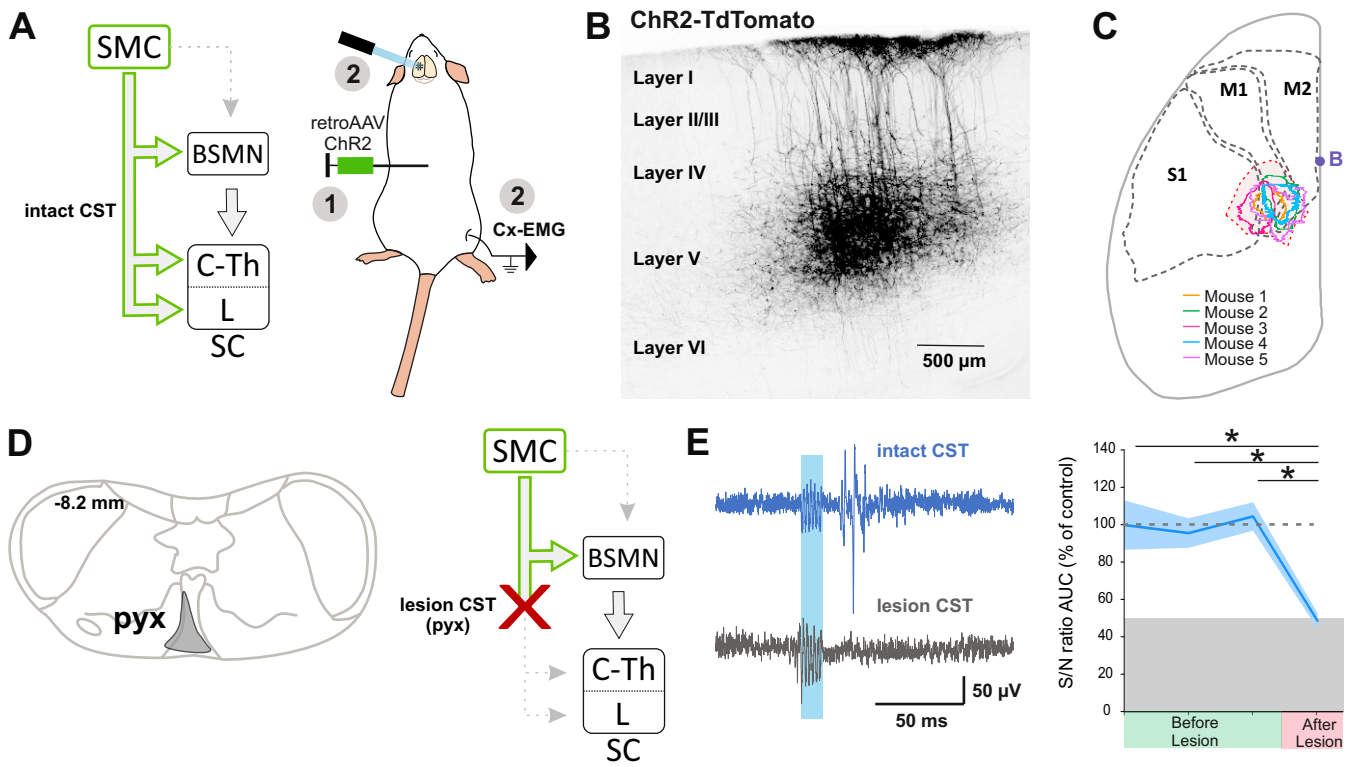

Figure 3. The corticospinal tract can encode muscular contractions.

A. *Left*, diagram illustrating corticospinal neurons and their collaterals expressing ChR2 after retrograde infection in the lumbar cord with a retroAAV. *Right*, experimental design: the photostimulation and EMG recording session took place at least 3 weeks after the infection.

B. Sagittal image from the sensorimotor cortex (Lateral= 0.68 mm), showing retrogradely labeled corticospinal neurons (expressing ChR2-TdTomato fluorescence).

C. Drawing of a cortex top view, showing the localization of retrogradely labeled corticospinal neurons in the 5 animals (solid lines). They are within the area functionally determined as inducing DRPs and EMGs in the hindlimb (dashed lines).

D. *Left*, drawing showing the extent of the pyramidal lesion in the animal whose recordings are illustrated in E. *Right*, diagram showing the supraspinal collaterals of ChR2-expressing CS neurons spared by the pyramidotomy. Systematic histological analysis of the pyramidotomies is presented in Figure 2 – Figure Supplement 1.

E. *Left*, cortically evoked EMG recordings before (blue) and after (grey) the pyramidal lesion. *Right,* the pyramidotomy abolishes cortically-evoked EMG ($p=0.012$, one-way ANOVA, n= 5 mice). Post-hoc test Holm-Sidak, $*P < 0.05$. Grey zone: noise level (see Methods). EMG Z-scores for individual mice before and after pyramidotomy are presented in Figure 2 – Figure Supplement 2.

The blue window on recording traces indicates light stimulation. SMC: sensorimotor cortex, BSMN: brain stem motor nuclei, C-Th: cervico-thoracic spinal cord, L-SC: Lumbo-sacral spinal cord.

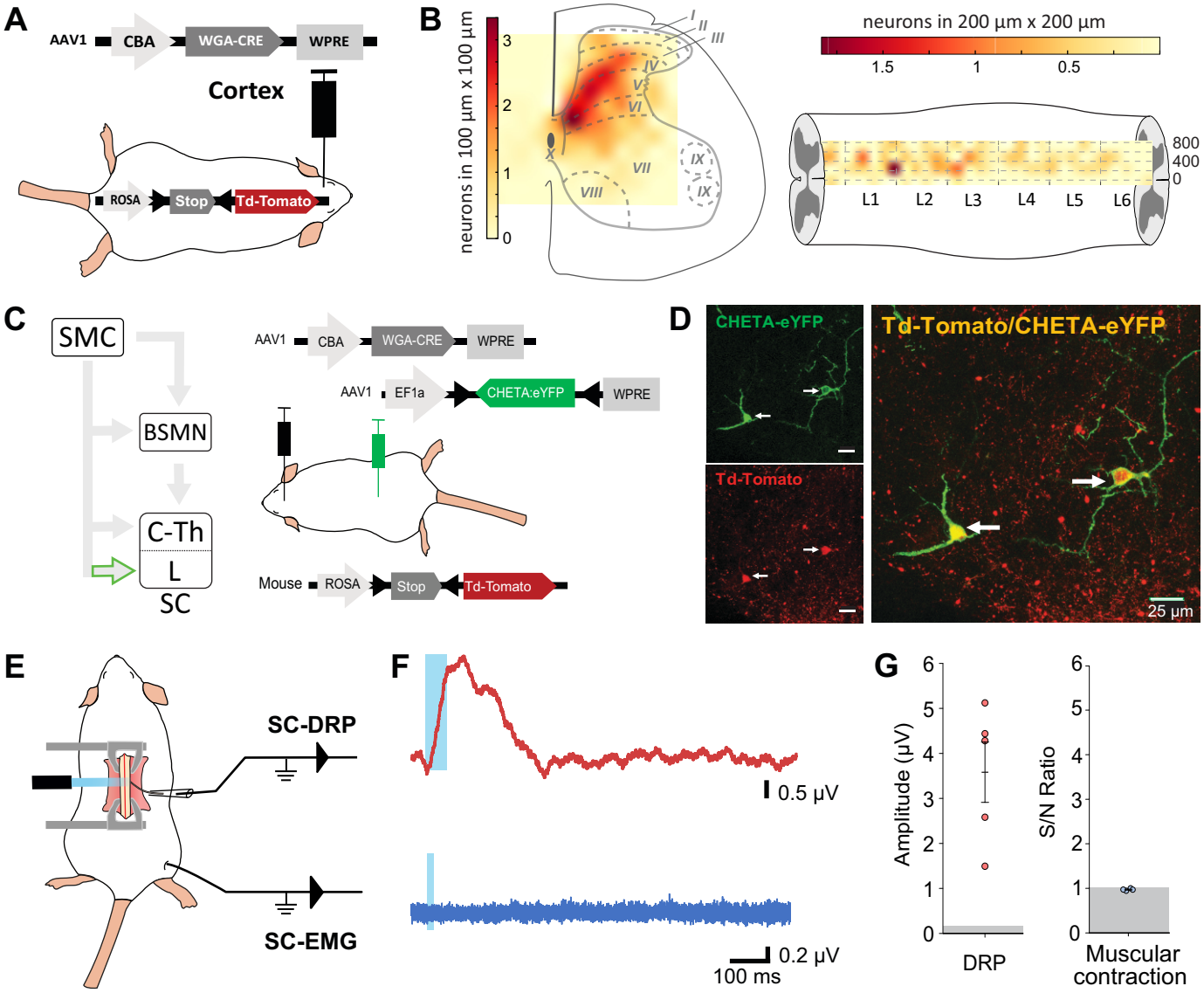

Figure 4. Lumbar corticospinal postsynaptic neurons encode DRPs but no movements.

A. Experimental design: the targets of the CST are labeled through a transynaptic approach consisting of AAV1-CBA-WGA-CRE injection in the hindlimb sensorimotor cortex of TdTomato-flex mice.

B. Localization of the spinal targets of the CST: heatmap showing the distribution of the neurons in the lumbar cord (6 mm long) projected into the transverse plane (average of 9 mice) (*left*) or horizontal plane (average of 6 mice) (*right*) plane.

C. *Left*, Diagram illustrating that only lumbar direct targets of the CST express CHETA in the following experiment. *Right*, Experimental design: TdTomato-flex mice received an injection of AAV1-CBA-WGA-CRE in the hindlimb sensorimotor cortex and an injection of AAV1-Efl-flex-CHETA-eYFP in the L4 spinal segment.

D. Photomicrographs (z projection of confocal images) from the dorsal horn of the spinal cord (laminae V/VI); the arrows point at two targets of the CST expressing TdTomato+ and CHETA-eYFP.

E. Experimental design illustrating spinal photostimulation of the lumbar targets of the CST.

F. Representative traces of DRP (red trace, average of 60 traces) and EMG (blue trace, average of 3 traces) recordings from the same animal after photostimulation of the lumbar targets of the CST (blue window).

G. Photostimulation of the lumbar targets of the CST induces DRPs (left) but no EMG signal (right). Grey zone: noise level (see Methods). EMG Z-scores for individual mice are presented in Figure 2 – Figure Supplement 2.

SMC: sensorimotor cortex, BSMN: brain stem motor nuclei, C-Th: cervico-thoracic spinal cord, L-SC:Lumbo-sacral spinal cord.